Strain-induced network chains damage in carbon black filled EPDM

Nicolas Candau, Oguzhan Oguz, Edith Peuvrel-Disdier, Jean-Luc Bouvard, Christophe Pradille, Noëlle Billon

Strain-Induced Network Chains Damage in Carbon Black Filled EPDM

Nicolas Candau [a,*,1], Oguzhan Oguz [b], Edith Peuvrel-Disdier [a], Jean-Luc Bouvard [a],

Christophe Pradille [c], Noelle Billon [a]

[a] Mines ParisTech, PSL Research University, CEMEF - Centre de Mise en Forme des Matériaux, UMR CNRS 7635, CS 10207, 06904 Sophia-Antipolis, France

[b] Laboratory of Macromolecular and Organic Materials (LMOM), Institute of Materials (IMX), Ecole Polytechnique Fédérale de Lausanne (EPFL), Station 12, 1015 Lausanne, Switzerland

[c] Mat-xper, 06560 Valbonne, France

[*]Corresponding author: nicolas.candau@epfl.ch

[1] Present address: Laboratory of Macromolecular and Organic Materials (LMOM), Institute of Materials (IMX), Ecole Polytechnique Fédérale de Lausanne (EPFL), Station 12, 1015 Lausanne, Switzerland

Abstract

This paper presents an experimental method to follow *in-situ* the chains network alteration of filled vulcanized rubbers induced by deformation. Macroscopic damage is first investigated on a series of EPDM by quantifying void fraction via Digital Image Correlation (DIC). *In-situ* DIC void fraction and the swollen pore fraction measured *ex situ*, i.e. on mechanically tested specimen, show analogous dependence on applied deformation. From such observation, Flory-Rehner equation is used by substituting fraction of swollen specimen by DIC void fraction to access to *in-situ* changes in network chains density, ν. Below the stretching ratio λ=3, reversible voids and accompanied by slight decrease of ν. Above λ=3, irreversible voids are associated with significant decrease of ν. Transition from reversible to irreversible voiding is finally ascribed to increased pore size of damaged elastically active chains network domains, as revealed by *ex situ* thermoporosimetry.

Keywords

Elastomers; Damage; Chains Network.

1. Introduction

Ethylene-propylene-diene-terpolymer rubber (EPDM) is one of the most attractive synthetic rubbers due to its outstanding resistance to aging and ozone combined with its strong ability to be extended with fillers and oil plasticizers. [1] It provides mechanical performances adapted to a large number of industrial applications. In tire sidewall, EPDM plays a major role to prevent dynamic propagation of crack due to its ozone resistance. [2,3] In nuclear power plants, EPDM serves as insulation of electric cables owing their ability to resist irradiation. [4] Recycling EPDM is then a crucial industrial challenge. [5] Because of weak penetration of devulcanization agents in the rubber matrix, mechanical devulcanization is a more promising route than chemical devulcanization. [6]

Mechanical devulcanization is assumed to convert mechanical work into molecular debonding or into an increase in temperature able to break some covalent bonds. In any case, the first step consists of physical breakage and dispersion into small pieces. Understanding the mechanisms at molecular scale responsible for this macroscopic failure is hence of great importance. The understanding of elementary processes involved in the deformation of given rubbers can be partly achieved by a systematic study at intermediate mesoscale to investigate the relationship between macroscopic observation and molecular mechanisms.

One approach consists of *in-situ* characterization of temperature and strain field during mechanical tests that combine Infrared thermography (IR) and Digital Image Correlation (DIC) respectively. These two techniques are often coupled to give insights on thermomechanical behaviour of polymeric systems. [7, 8, 9] However, their combination to access potential damage is not systematically discussed. Damage is a dilatational mechanism, associated with void creation and hence generates a raise of volumetric strain accessible by DIC. [10,11] Part of mechanical

dissipation originates from damage, and is further converted into heat. [12] In rubbery materials, energy dissipation has an essential role in fracture mechanisms [13] and damage can be distinguished from other dissipative contributions as proposed in ref. [14]

At molecular scale, filled vulcanized rubbers contain various types of network bonds such as chemical cross-links, physical rubber-filler bonds, chains entanglements. The structure and heterogeneities of such complex network in carbon-black filled EPDM has been widely discussed. [15,16] The associated damage can find various origins: chains scission, sulphur-bond breakage, decohesion at filler-rubber interface, filler-filler rupture, [17] molecules slippage at fillers surface. [18]

Fillers and vulcanization systems both have a dominant role in damage mechanisms in filled vulcanized rubber. Rigid fillers significantly accelerate voiding via strain amplification, and occurs at filler/rubber interface due to a high hydrostatic stress. [11,19, 20] Vulcanization, by modifying the average end-to-end distance between chains, controls the local chains extension upon macroscopic strain which, in turn, tends to increase elastic strain energy associated with void nucleation that subsequently grows and transforms into cracks. [19, 20,21]

The relationship between chains network damage and macroscopic mechanical behaviour of filled vulcanized rubber is however difficult to clarify as it strongly depends on the filler system (nature, size, spatial distribution), the rubber system [22] (chemical nature, molecular weight, entanglements density), the filler-rubber interface, the vulcanization system (peroxide or sulphur vulcanized with mono, or poly sulfidic bonds), and the experimental conditions [23] (temperature, strain rate). Mullins suggested that voids formed around Zn oxides clusters resulting from incomplete vulcanization are mainly responsible for voiding during loading at high strain rate. [24] Swelling of filled vulcanized Natural Rubber (NR) and Styrene-Butadiene Rubber (SBR) that

undergo single loading reveal relative decrease of 15% of network chains density, ν, [22,23] compare to the value for virgin rubber for a strain rate of 0.4 s^{-1}. More drastic thermo-mechanical solicitations like High Shear Mixing (HSM) yield in a decrease of ν by more than 70%, partially due to chemical crosslink breakage. [6] Due to the significant modification of chains network during the mechanical solicitation of rubber systems, many physically based models have been developed like mechanochemistry that incorporates strain induced network alteration. [25,26,27,28]

In spite of a large number of experimental studies and mechanical modelling, relationship between network chains damage and macroscopic damage in rubbers is still not systematically investigated and requires an adapted experimental methodology. To this aim, a multi-scale approach is used in this paper. Strain and thermal fields measured on the local surface of the specimens are tracked *in situ*, i.e. during tensile cycles. Three vulcanized EPDM and one unvulcanized EPDM are studied. Their network chain densities are measured *ex situ* by swelling. We highlight an equivalence between void fraction obtained by DIC and swollen pores fraction measured by swelling and propose a method to identify the alteration of chains network *in situ*, i.e. during the rubber deformation. Chains network damage has been found to be associated with a transition from reversible to irreversible voiding mechanisms at a certain stretching ratio. We ascribed such transition to thermal stability of irreversible cavities consistent with an observed rise in size of damaged areas of rubber network measured by DSC thermoporosimetry.

2. Materials and experiments

2.1. Materials composition and processing

The materials are extended oil carbon black filled EPDM (Keltan 5470) obtained by sulphur vulcanization of the gum. They contain 70% in mass of Ethylene and 4.6% of ethylidene norbornene (ENB). The crystalline fraction estimated from Differential Scanning Calorimetry

(DSC) is found less than 3% wt. for all materials. All materials contain 80 phr (80g per 100 g of rubber) of carbon black (N550), 65 phr of paraffin oil, 4 phr of calcium oxide, 5 phr of zinc oxide, 1 phr of stearine, 2 phr of PE 6 4000. The vulcanization components are the following: 1.2phr of sulfur (75%), 1 phr of mercaptobenzothiazole (MBT 75%), 0.8% phr of mercaptobenzothiazole disulfide (MBTS 75%), 1.2 phr of N-cyclohexyl-2-benzothiazolesulfenamide (CBS 75%), 1.5 phr of zinc dialkyl dithiophosphate (ZDTP 70%). The rubbers are processed in an internal mixer. Sample sheets are then obtained by curing in a hot press at high temperature. As shown in table 1, different curing conditions are used to obtain vulcanized rubbers with different network chain densities, *ν*. EPDM-1 and EPDM-3 have been cured at 140°C for 15 minutes and 255 minutes respectively so that the torque reaches 50% and 100% of maximum RPA. EPDM-2 has been cured at 170°C for 15 minutes so that the torque reaches 100% of maximum RPA. The ratio of accelerators over sulphur corresponds to efficient vulcanization system (EV), where the proportion of mono and disulfidic crosslinks is higher than for conventional vulcanization systems (CONV). Dumbbell-shaped samples, with a 15 mm gauge length (L_0), 6 mm thickness and 10 mm width, are then machined for mechanical testing.

Material Code	EPDM-0	EPDM-1	EPDM-2	EPDM-3
Curing temperature (°C)	X	140	170	140
Curing time (min)	X	15	15	255
ν ($x10^{-4}$mol.cm^{-3})	No meas.	1.34	2.85	3.67

Table 1. Recipes and network chain density, ν, of elastically active chains estimated from swelling measurements (in 10^{-4} mol.cm^{-3}). ν has not been measured in the case of EPDM-0 as it is transforms into a gel soluble in cyclohexane during swelling experiments.

2.2. Temperature and strain field measurement

Mechanical tests are performed on an electromechanical tensile test machine INSTRON 5960. Rubber samples are stretched and unstretched at room temperature. The nominal tensile strain rate chosen for these tests is $1s^{-1}$. The displacement fields on the front and side faces of the sample are recorded using a four-cameras system which consists of two-pairs systems (Figure 1). Like for a single stereovision-system, each camera pair is set up independently of the other one. Both systems are then placed in the same coordinate system using a calibration target. A low sampling rate of cameras (10 Hz) is chosen to ensure a low nominal strain increment between two images and make strain tracking more accurate. Front and side surfaces of the samples are coated with a white spray paint to generate a random speckle pattern. The series of images are post-processed using VIC-3D software package. [29] 3D DIC displacement data is converted into strain values with λ_1 the stretching ratio in the tensile direction, λ_2 and λ_3 are the transversal stretching ratios in the directions of the sample width and thickness respectively. More details on the choice of DIC parameters are provided in ref. [30]

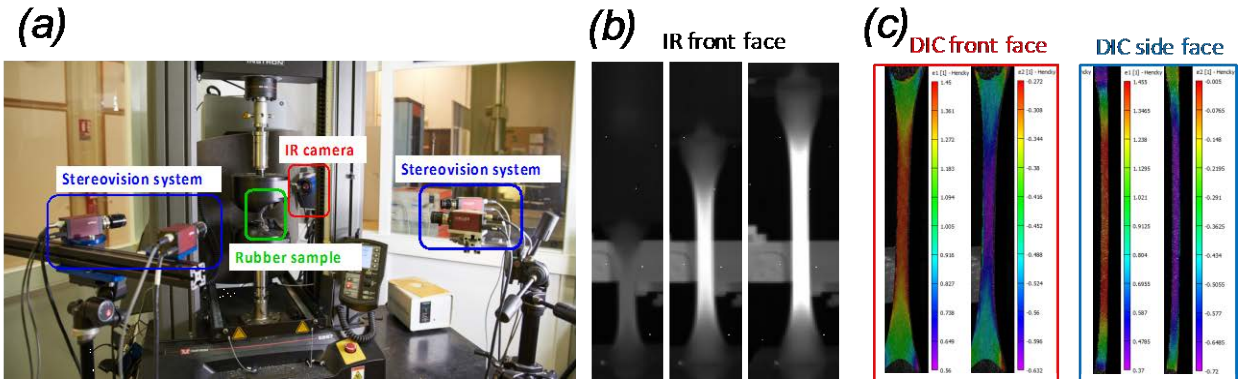

Figure 1. *(a)* Experimental thermomechanical set-up based on two independent stereo-vision systems to measure simultaneously strain fields on front and side surfaces of specimen and infra-red camera to measure temperature field on the front face of same specimen, *(b)* temperature field measured on the front face at various strains (white area indicates highest temperature), *(c)* longitudinal and transverse strain fields analysed on front and side faces of the specimen for a given macroscopic deformation.

The transversal and longitudinal strains are homogeneous in the center of the sample and significantly decrease close to the clamping zones (Figure 1c). The strain fields in both front and side surfaces are obtained from a region of interest (ROI) in the central part of the sample. The true stress is defined as the ratio between the applied force F and the specimen cross section:

$$\sigma_T = \frac{F}{L_0 e_0 \lambda_2 \lambda_3} \quad (1)$$

where L_0 is the initial length and e_0 the initial width. The volumetric strain $\Delta V/V_0$ is defined as:

$$\Delta V/V_0 = \lambda_1 \lambda_2 \lambda_3 - 1 \quad (2)$$

For some tests performed at the highest stretching ratios, strain field in the thickness of the sample can be difficult to extract, due to strong reduction of thickness and too few pixels to be analysed. However, we found that the relationship $\varepsilon_3=1.1\varepsilon_2$ between transverse deformations remains constant during the specimen axial deformation. Such weak transversal anisotropy is expected from processing conditions (calendaring), and consistent with previous observations. [31] Volumetric strain can then be deduced for the highest stretching ratios assuming such relation being verified.

Trace of self-heating generated in the sample is recorded on its surface during the deformation using FLIR SC5000 camera. Temperature field is analysed on the front face of the specimen with ALTAIR software in the same ROI than for DIC analysis. Rubber samples stretched at different maximum strains are then stored after unloading at room temperature before performing ex situ swelling and thermoporosimetry.

2.3. Swelling

Swelling experiments using cyclohexane as a solvent are performed to determine the network chains density of the undeformed and mechanically tested EPDM specimens. Each sample is immersed in solvent for 72 h and the solvent is changed every 24 h. After 72 h the swollen mass of each sample (m_s) is measured. Then, the samples are placed in an oven under vacuum at 70°C during 6 h to remove the solvent. The mass of the dry samples (m_d) are then measured. The swelling ratio of the specimen *Q* is calculated as follows:

$$Q = \frac{\frac{m_s - m_d}{\rho_{solv}}}{\frac{m_s - m_d}{\rho_{solv}} + \frac{m_d}{\rho}} \tag{3}$$

With ρ_{solv}=0.778g.cm^{-3} is the density of the solvent and ρ the density of dry rubber specimen after de-swelling under vacuum. Like for DIC volumetric strain, volumetric strain for swelling experiments $\Delta Q/Q_0$ is defined as:

$$\frac{\Delta Q(\lambda)}{Q_0} = \frac{Q(\lambda) - Q_0}{Q_0} \tag{4}$$

with $Q(\lambda)$ denotes the swelling ratio of a specimen mechanically tested up to λ and $Q_0 = Q(\lambda = 1)$ the swelling ratio of a virgin specimen (undeformed). For filled compounds the Kraus correction [33] is used to account for the contribution of filler in swelling ratio. Q_r is the swelling ratio of the rubber matrix defined as follows:

$$Q_r = \frac{Q - \varphi}{1 - \varphi} \tag{5}$$

with φ is the volume fraction of fillers calculated as:

$$\varphi = \frac{\frac{m_c}{\rho_c}}{\frac{m_c}{\rho_c} + \frac{m_{pol}}{\rho_{pol}}} \quad (6)$$

m_c and ρ_c=1.87g.cm^{-3} are the dried mass and density of carbon black respectively. m_{pol} and ρ_{pol} are the dried mass and density of polymer respectively measured after deswelling in vacuum. Krauss correction in Equation 5 assumes non-adhesion of the fillers to the rubbery matrix, hence creating vacuole. Such assumption is realistic in the frame of our study because swelling is performed on both virgin and mechanically tested specimen whose damage are partly ascribed to decohesion mechanisms, as will be discussed in the following. The average network chain density is then calculated from swelling experiments and the Flory-Rehner equation: [32]

$$v = \frac{ln(1 - v_2) + v_2 + \chi_1 {v_2}^2}{V_1(-{v_2}^{\frac{1}{3}} + \frac{2}{f} v_2)} \quad (7)$$

With $v_2 = 1/Q_r$. V_1=108 cm^3/mol^{-1} is the molar volume of the solvent (cyclohexane), χ_1 is the Flory-Huggins polymer solvent dimensionless interaction term (χ_1 is equal to 0.353 for the EPDM-toluene system). The ratio *2/f* is associated with the phantom model that assumes spatial fluctuation of crosslinks (non-affine) used for high deformation ratios. *f*, the crosslink functionality, is chosen equal to 4.

2.4. Thermoporosimetry

When crystallized, solvent molecules constrained to small volumes form relatively small crystallites and which therefore exhibit lower melting temperatures than the infinite crystal. Practically, NR samples are put into a solvent (cyclohexane) during 72 h to reach the swelling equilibrium. They are then carefully extracted and put into an aluminium crucible. A Perkin Elmer Pyris diamond DSC is used. First, the sample is cooled down to - 50°C at 10°C/min

followed by an isothermal step at –50°C during 2 min. The sample is then heated at 10°C.min^{-1} up to 30°C. When temperature increases, the first peaks (or series of peaks) that appear corresponds to the melting of the cyclohexane entrapped in the network. The last peak (around 10°C) corresponds to the melting point of free cyclohexane (i.e. in excess). Melting peaks are deconvoluted by use of asymmetric Lorentzian functions (Figure S4a). After removal of free solvent melting peak (Figure S4b), the intensity is normalized by the swollen weight. The procedure is described in reference [34]. Based on Gibbs-Thompson equation, the pore size L is related to the melting temperature T_m by:

$$T_m^\circ - Tm = \frac{2\sigma_{SL} T_m^\circ}{L\Delta H_f f} \quad (8)$$

With σ_{SL} is the solid-liquid surface energy, T_m° is the melting temperature of the free solvent and $\Delta H_f = 6.3\, J.g^{-1}$ is the melting enthalpy of the solvent. The normalized pore size is given by:

$$\frac{L}{L_f} = \frac{T_m{}^0 - T_f}{T_m{}^0 - T} \quad (9)$$

With T_f and L_f correspond to the melting temperature and the size of the largest pores entrapped in the network respectively. It should be noted that the absolute value of L_f is not accessible from thermoporosimetry. Hence in the following, the normalized pore size L/L_f, instead the absolute pore size L, will be employed to discuss on the effect of both crosslink density and stretching ratio on pores size. After derivation of equation 9, the normalized intensity distribution of the pore size is given by:

$$I_n = \frac{1}{m}\frac{dH}{dT}\frac{\left({T_m}^0 - T\right)^2}{L_f} \quad (10)$$

L_f value being unknown, the intensity $I=L_fI_n$ is hence plotted instead I_n to account for the pore size distribution. An example of the plot $I=f(L/L_f)$ is provided in Figure S4c. The average normalized pore size is then calculated as the L/L_f value associated with half of the area under the normalized signal (denoted by the vertical line in Figure S4c).

2.5. Scanning electron microscopy (SEM)

Fractured surfaces of specimens subjected to tensile test were analysed by a Carl Zeiss AG SUPRA 40 electron scanning microscope. Electrons are collected by in-lens detector. A working distance of 5 mm and an acceleration voltage is 3keV are used. Samples are coated with carbon to avoid charging. Working distance of 9.9 mm is used for EDX analysis and the determination of the chemical composition.

3. Results and discussion

3.1. Macroscopic damage via strain-induced thermal and volume changes

Thermomechanical characterization of unvulcanized and vulcanized filled rubbers subjected to mechanical cycles up to various stretching ratios, λ, and at high strain rate (1 s^{-1}) has been performed (Figure 2 and Supplementary Figures S1-S3). Stress-stretching ratio loading-unloading curves exhibit classical mechanical hysteresis (Figure 2a, Supplementary Figures S1a-S3a). Evidence for energy dissipation exists but strain appears to be mostly geometrically reversible. Such energy is converted into heat. Figures 2b and Supplementary Figures S1b-S3b display the evolution of self-heating with the stretching ratio. Self-heating, ΔT, gradually

increases on the sample surface during loading and decreases during unloading with positive hysteresis. A negative loop is observed in all EPDM for λ>4.

These dissipative mechanisms can find several origins. First, it should be noted that the contribution of crystal plasticity to dissipative mechanisms is negligible due to the weak crystalline fraction (less than 3% wt.) and strain-induced crystallization is unlikely due to paraffin oil that impedes molecular ordering, as shown in polyisoprene [35] and cis-1,4 polybutadiene [36]. Dissipative mechanisms are hence rather ascribed to a high viscosity owing the presence of fillers [37,38] as well as the damage associated with voiding. [14]

Damage can occur due to strain amplification and stress concentration in the vicinity of fillers and filled rubbers generally exhibit large amount of voids. [39,21] Digital Image Correlation (DIC) is used to measure volumetric strain that characterizes voiding volume fraction depending on applied deformation (Figure 2c, Figures S1c-S3c). Below λ =1.5, the absence of volumetric strain attests for rubber incompressibility in the elastic regime (ν = 0.499). [40] However, above λ =1.5, volumetric strain significantly increases as a function of stretching ratio, proving non-isochoric deformation. For λ <3, increase in volumetric strain could be reversible, though not elastic. For λ >3, volumetric strain is not recovered within the duration of test. This suggests the appearance of irreversible deformation mechanisms is likely associated with voids, which could not be closed upon unloading.

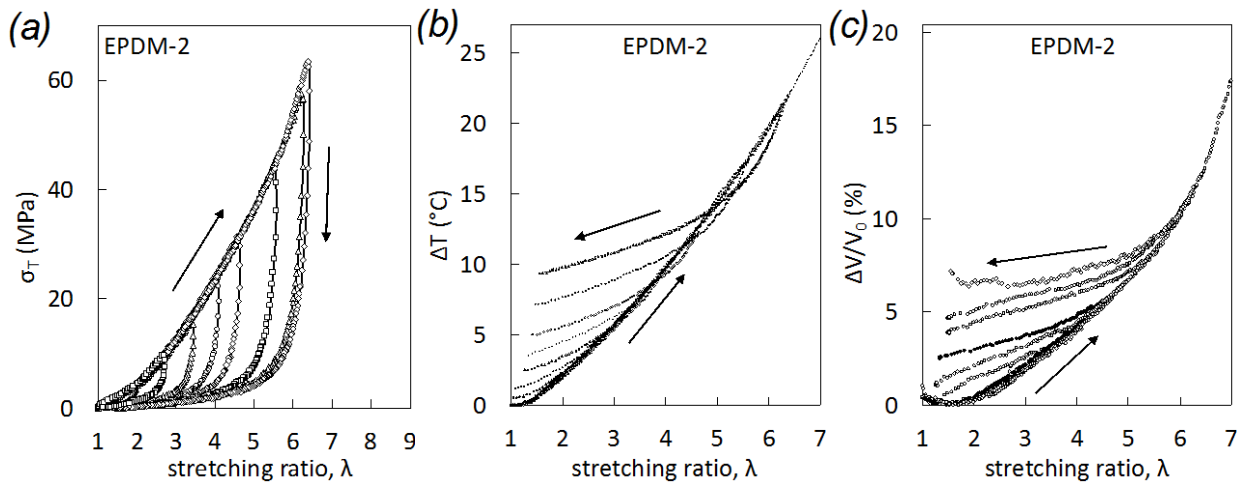

Figure 2. True stress *(a)*, self-heating *(b)* and volumetric strain *(c)* during uniaxial cyclic test performed on EPDM-2 at room temperature and at the strain rate $1s^{-1}$.

Studying the relationship between mechanical energy and self-heating is required to identify viscous and damage contributions to dissipative mechanisms (Figure 3). Thermomechanical coupling describes reversible and irreversible deformation processes. The integration of reversible mechanisms to time over one cycle is zero. If adiabatic conditions prevail, as in the case of high-strain rate loading, and the thermo-elastic coupling is neglected, the heat equation integrated with time can be written as:

$$\rho C_p \Delta T = E_{diss} = E_1 + E_2 \qquad (11)$$

where C_p, is the heat capacity ($J.g^{-1}{}^{\circ}C^{-1}$) and ρ is the bulk density ($g.cm^{-3}$) of EPDM materials. E_{diss} is the energy dissipated over a cycle, measured as the difference of area under the loading and unloading curves. E_1 and E_2 are the heat production due to mechanical irreversibility, bulk viscosity and damage respectively. E_{diss} and ΔT both increase with stretching ratio and network chains density (Figure 3a-b). In a certain energy range (from 0 to 15 $MJ.m^{-3}$), relationship between ΔT and E_{diss} follows a unique curve regardless of the network chains density, ν (Figure 3c). Assuming similar C_p, and ρ for all tested materials, this means that the same quantity of

mechanical energy is transferred into heat, and that respective contributions of viscosity and damage to dissipation do not depend on the network chains density for this energy range. For a higher energy range (above 15 $MJ.m^{-3}$), slight upturns of self-heating are observed for the vulcanized EPDM (Figure 3c). This attests for a predominance of one of the two main contributions to heat dissipation, which is accelerated with increased network chains density. This contribution should be damage because of higher stress concentration in the rubbery matrix due to higher density of sulphur-bonds and trapped entanglements. Contrarily, such upturn is prevented in the unvulcanized EPDM which can accommodate the stress up to very large deformation owing strong viscosity contribution to mechanical dissipation, via disentanglement or filler network deformation.

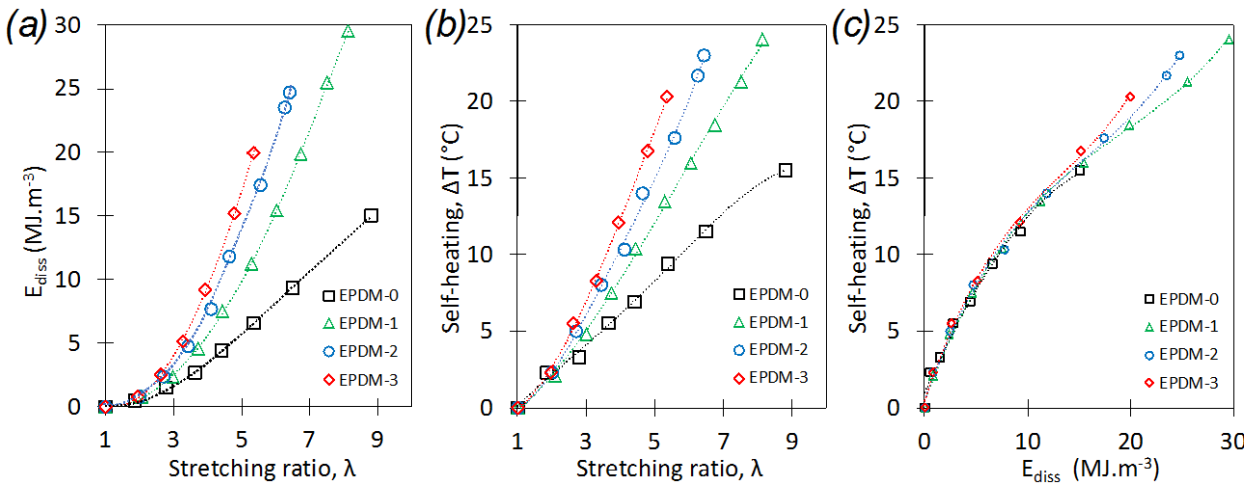

Figure 3. *(a)* dissipated energy vs. stretching ratio, *(b)* self-heating accumulated at maximum strain during loading, λ,vs. stretching ratio, *(c)* self-heating vs. dissipated energy for EPDM-0, EPDM-1, EPDM-2 and EPDM-3. Dissipated energy is calculated from the area under the curve of the cyclic tests (Figure 2a, Supplementary Figures S1a-S3a).

Relationship between damage mechanisms and network chains density, ν, is investigated by comparing volumetric strain behaviour for all EPDM. True stress, volumetric strain, tangent modulus and volumetric strain rate are plotted in Figure 4. Expectedly, tensile strength increases

with ν (Figure 4a), obtained by increasing curing temperature: no vulcanization (EPDM-0), vulcanization at 140°C (EPDM-1) and vulcanization at 170°C (EPDM-2). However, tensile strength levels off for the rubber with the highest crosslink density (EPDM-3). This can be explained by polysulfidic bonds, that favour chains mobility yielding higher tensile strength, [41] predominant at low curing times (EPDM-1 and EPDM-2) but which transform into mono and disulfidic bonds [42] with increasing curing time (EPDM-3) yielding in decreased tensile strength.

The tangent modulus provides an estimate of stiffness at a given stretching ratio (Figure 4b). It first decreases with stretching ratio which is consistent with Gaussian behaviour, $\sigma = E/3\ (\lambda - 1/\lambda^2)$, E being the elastic modulus. At an inflexion point around λ=1.5, experimental trend deviates from the Gaussian theory. The stretching ratio at inflexion point can be interpreted as the macroscopic stretching ratio associated with the limit extensibility of the shortest chains that contribute to the elastically active network. [43] This stretching ratio being close for all materials, similar length of the shortest chains between bonds of the network is expected. While swelling provides an average value of chains length, network heterogeneities are expected in sulphur-cured filled EPDM due to numerous macromolecular interactions, [15,16] justifying a certain distribution of chains length as also shown in our materials by thermoporosimetry experiments (see section 2.4, Figure 10 and Supplementary Figure S4). In the case of unvulcanized EPDM-0, the chains network elasticity is activated via trapped entanglements and rubber-filler interactions.

Volumetric strain onset (Figure 4d) is concomitant to stretching ratio at inflexion point (Figure 4b). Onset of volumetric strain is hence assumed to be associated with breakage of short chains domains due to their high level of stress concentration. Voiding onset occurs at early stage of deformation for unvulcanized EPDM-0. Due to the absence of moulding and curing step in hot-

press, pre-existing stable micro-voids before mechanical testing is expected to favour void growth in that material.

Above the stretching ratio at inflexion point, volumetric strain increases faster with increased average network chains density (Figure 4c-d). Such trend is consistent with previous findings from the literature. [19,20] Increased volumetric strain up to failure traduces damage that involves domains containing longer and longer chains successively stretched up to breakage. Hence, as suggested above, contrarily to volumetric strain onset dominated by local short chains damage, damage at larger strains is more dominated by the alteration of the average network chains density (Table 1). One might note that the maximum volumetric strain is observed for the unvulcanized EPDM (EPDM-0) owing its ability to undergo large strain without macroscopic failure. Total void volume fraction in that material is even likely underestimated because voids that pre-exist to stretching are not counted in volumetric strain.

Strain to failure decreases by increasing the network chains density, ν. In the strain range preceding macroscopic failure of vulcanized EPDM, tangent modulus upturn indicates strain hardening (arrows in Figure 4b) while unvulcanized EPDM is subjected to strain softening. These upturns are concomitant with volumetric strain rate upturns observed in vulcanized EPDM (arrows in Figure 4d) indicating a dramatic acceleration of damage. Such acceleration can partly explain previously observed heat upturns that occur at same deformation levels (Figure 3c).

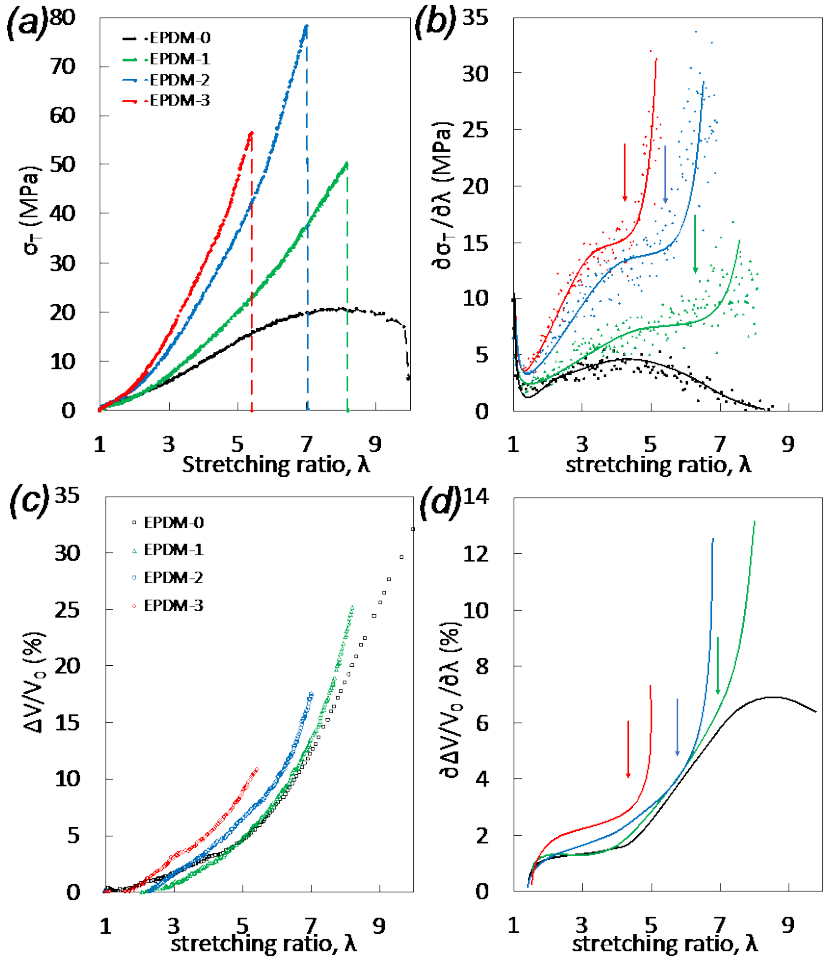

Figure 4. *(a)* True stress, *(b)* tangent modulus (calculated as the derivative of stress over strain) vs. stretching ratio, *(c)* volumetric strain vs. stretching ratio and *(d)* rate of volumetric strain (calculated as the derivative of volumetric strain over strain) vs. stretching ratio. Arrows indicate upturns related to slope changes of stress and volumetric strain.

The permanent longitudinal and volumetric strain obtained after loading-unloading tests are presented in Figure 5. Fully reversible volumetric strain is observed for an applied stretching ratio λ <3 independently of the tested EPDM specimens (Figure 5a). For λ>3, volumetric strain becomes irreversible within the experimental time suggesting that voids remain open. The transition from reversible to irreversible voiding mechanisms is associated with a change in the slope of permanent longitudinal deformation at $\lambda \approx 3$ (Figure 5b) and can be explained by the contribution of deformed domains containing voids to the macroscopic longitudinal deformation. The following section will provide an interpretation of such transition at network chains scale.

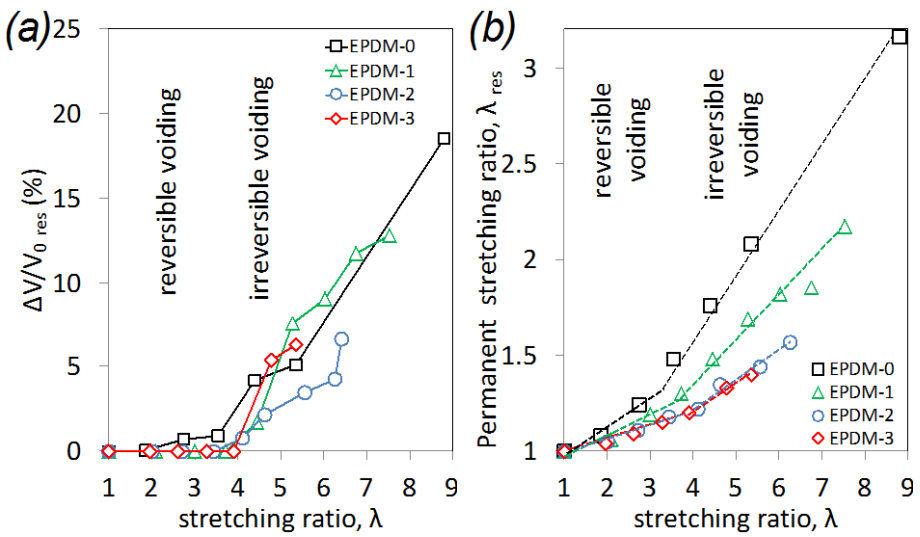

Figure 5. *(a)* Volumetric strain and *(b)* Stretching ratio measured right after unloading for EPDM-0, EPDM-1, EPDM-2 and EPDM-3 showing a transition from reversible to irreversible damage at λ=3 within the experimental time.

3.2. Damage at micro and molecular scale

Damage at micro and molecular scales are accessible via the observation of fractured surface (Figure 6) and solvent swelling behaviour (Figure 7-10). SEM images of fractured surface of mechanically tested specimen (EPDM-2) show fracture lines propagated in the rubbery matrix (Figure 6a). Observations at high magnitude reveal hundred nanometre sized carbon black fillers well dispersed in the rubbery matrix (Figure 6b). Fracture propagation lines are somewhat deviated by the fillers, that mostly remain attached to the rubber matrix while a few of them are debonded. Rigid micro-particles of ZnO and CaO (Figure 6a,c) are residual components resulting from the incomplete vulcanization. Micro-voids in the vicinity of these clusters can result from their decohesion to the rubbery matrix and have been suggested to be initiators of macroscopic failure in filled rubber when subjected to fatigue. [21] Decohesion of fillers and rigid clusters partly contribute to voiding mechanisms quantified by volumetric strain (Figure 4c). Decohesion creates vacuoles surrounding rigid clusters or fillers which would then grow into larger voids.

Additionally, void nucleation is also expected to occur in the rubber matrix constrained between the filler aggregates due to high hydrostatic stress. [44] Regarding large voids fractions (Figure 4c), voiding does not remain localized at filler/rubber interface, but void growth should occur and necessarily accompanied by alteration of chains network of the rubber matrix as discussed in the following.

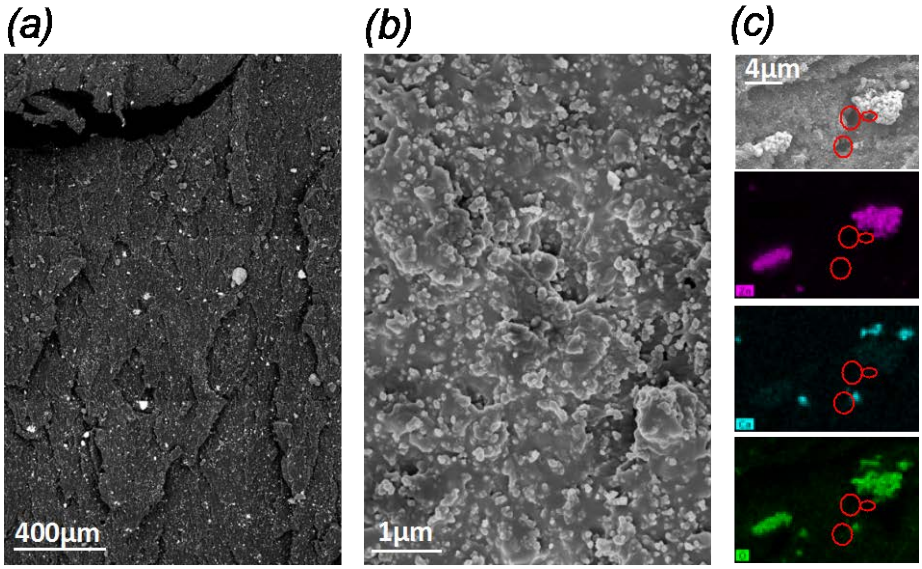

Figure 6. *(a),(b)* SEM images of cross-section of fractured EPDM-2 sample, *(c)* SEM-EDX images on sample EPDM-2. In red are highlighted the principal zones showing cavities. Zinc, Calcium and Oxygen have been identified with EDX mapping in zones containing cavities.

Increased DIC volumetric strain with applied deformation should translate voiding mechanisms at molecular and network chains scale. To assess this, the fraction of porosities at network chains scale is quantified by swelling (Figures 7-8) and DSC thermoporosimetry (Figures 9-10) performed on vulcanized materials mechanically tested up to different λ. Swelling ratio first slightly increases up to a critical value λ=3 for all vulcanized EPDM (Figure 7a). Above such critical value, slopes break-down indicates higher increase of Q traducing an overall increase of volume fraction of swollen areas in the specimens with applied deformation. The slopes change coincides with transition from reversible to irreversible voiding (Figure 5a). Q tends to level off

for EPDM-1 and EPDM-3 and even decrease for EPDM-2 for the higher deformations. To further evaluate the relationship between DIC volumetric strain and swelling behaviour, we define a volumetric strain for swelling experiments, $\Delta Q/Q_0$, as defined in equation 4 in section 2.3, with Q the swelling ratio of a specimen that experiences mechanical testing and Q_0 the swelling ratio of un-tested material. $\Delta Q/Q_0$ is plotted versus $\Delta V/V_0$ obtained at various λ (unfilled data points, Figure 7b). $\Delta Q/Q_0$ follows $\Delta V/V_0$ regardless of the tested materials up to a value around 10%. For values of $\Delta V/V_0$ higher than 10%, $\Delta Q/Q_0$ reaches a threshold. Several sources of error can be identified when measuring swelling ratio on stretched specimen. First, decohesion between clusters and rubbery matrix (Figure 6c) can yield to an overestimate of rubber swelling due to creation of vacuoles at cluster interface. [45] Regarding their low volume fraction, their impact on $Q(\lambda)$ and $\Delta Q/Q_0$ is negligible here. More important is the presence of voids in specimens stretched up to λ >3 (figure 5a) that are maintained when unloaded. Assuming that solvent first fills these stable cavities but does not participate in rubber swelling, the corrected swelling that accounts for the presence of pre-existing voids is given by:

$$Q_{corr}(\lambda) = \frac{Q(\lambda) - \left.\frac{\Delta V}{V_0}\right|_{res}}{1 - \left.\frac{\Delta V}{V_0}\right|_{res}} \tag{12}$$

$\Delta Q_{corr}/Q_0$ is then calculated with equation 4 (see section 2.3) by substituting $Q(\lambda)$ by $Q_{corr}(\lambda)$, with $\left.\frac{\Delta V}{V_0}\right|_{res}$ is the residual (or permanent) volumetric strain provided in Figure 5a. Corrected values of volumetric strain $\Delta Q_{corr}/Q_0$ reasonably follow $\Delta V/V_0$. (filled data points, Figure 7b), showing DIC voids fraction and swollen pores fraction to comparably describe voiding mechanisms.

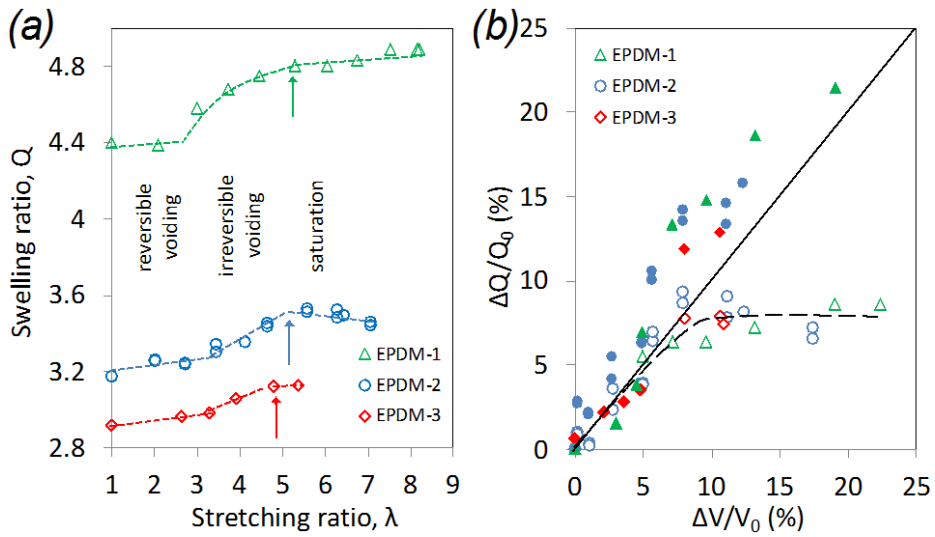

Figure 7. *(a)* Swelling ratio measured on EPDM-1, EPDM-2 and EPDM-3, versus maximum stretching ratio that specimens have undergone during mechanical testing, *(b)* relative swelling ratio calculated from figure 7a versus relative volumetric strain estimated from DIC for EPDM-1, EPDM-2 and EPDM-3. The continuous line is a plot of $\Delta Q/Q_0 = \Delta V/V_0$. Dotted line is a guide for the eyes and follows the experimental trend (unfilled data).

The network chains density $\nu(\lambda)$ shown in Figure 8a (unfilled data) is estimated from $Q(\lambda)$ (Figure 7a) by using equations 3-7. ν progressively decreases and stabilizes or even increases in the case of EPDM-2. Using the previously described equivalence between DIC voiding and swollen pores, an estimate of $\nu(\lambda)$ via $\Delta V/V_0$ obtained by DIC can be provided by substituting Q by V in equations 3-7 and assuming $v_2 = 1/V_r$, with V_r is the "dry" volume of rubber that contain porosities (instead of swollen volume for the calculation of Q_r) at a given deformation. The obtained ν is found to regularly decrease with applied stretching ratio (Figure 8a, continuous trends) and well follows ν estimated by swelling up to values indicated by arrows. For deformations above arrows, trends deviate because permanent voids are not considered in the calculation of ν by swelling. The correction proposed in eq. 10 is applied by using Q_{corr} instead of Q and the corrected ν are plotted in Figure 8b (filled data) and found consistent with ν obtained by DIC (trend lines, Figure 8b).

From both approaches, namely DIC and swelling, network chains density, ν, is found to significantly decrease with applied deformation up to failure with a maximum relative decrease of -40%, -35% and -23% for EPDM-1, EPDM-2 and EPDM-3 respectively, consistent with void fraction of 24%, 17% and 11% for the same materials (Figure 4c).

In addition to loss of chemical and physical bonds at filler/rubber interface, large decrease in ν is necessarily accompanied by sulphur-bond breakage and/or chains scission in the rubbery matrix. The entanglement density of EPDM being equal to 2-2.4.10^{-4} mol.cm^{-3},[46] EPDM-2 and EPDM-3 are over-crosslinked. It means that their average network chains densities which comprise both chemical crosslinks and trapped entanglements mostly occurs by sulphur bond breakage. In specific case of EPDM-2, average network chains density decreases down to entanglement density, suggesting more entanglement breakage to be activated at large deformation for such material. Contrarily, EPDM-1 is under-crosslinked and damage of chains network is mostly associated with chain scission.

In conclusion, the chains network alteration upon stretching is accompanied by sulphur bond breakage and chain scission that induce the creation of reversible voids in the first stages of deformation (λ<3) and irreversible voids at higher deformation (λ>3). Such transition should be interpreted via more quantitative analysis of void size.

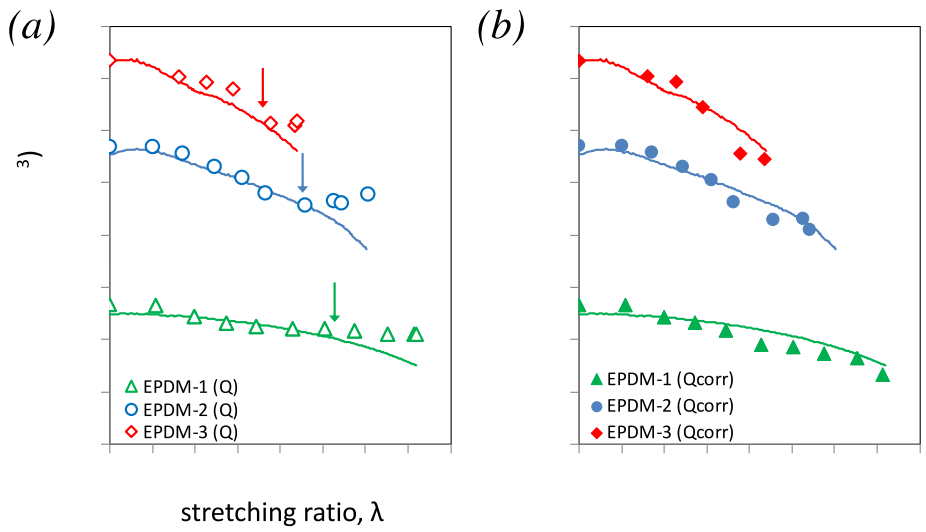

Figure 8. Network chain density, ν, estimated by swelling (data points) versus stretching ratio for EPDM-1, EPDM-2 and EPDM-3 mechanically tested at different maximum strain, without residual volumetric strain correction *(a)*, with corrections *(b)*. Calculations of ν are described in section 2.3 and corrections performed with the use of equ. 12. ν calculated by DIC volumetric strain is plotted with continuous lines. Arrows indicate deviation between swelling and DIC methods. Corrections to measure Qc_{orr} using equation 12 can only be applied for specimen cyclically stretched, i.e. for which permanent volumetric strain is measured. Hence, such method is not applicable for specimen stretched up to failure (data at highest stretching ratios in figure 8a).

DSC thermoporosimetry is used to provide an analyse of the size of damaged domains independently of previously described swelling experiments. Such method is based on the principle that solvent molecules crystallized in a rubber matrix are constrained to small volumes and form only relatively small crystallites. Owing to a decrease of the chemical potential of solvent molecules in polymer solution [47], they exhibit melting temperature depression. Crystallized swollen EPDM previously stretched at different λ are heated to access the melting behaviour as shown in Figure 9. Heating of EPDM-2 and EPDM-3 specimens is characterized by three endothermic peaks: $T_{m,1}$ and $T_{m,2}$ due to trapped solvent and $T_m^0 = 10°C$ the melting temperature of infinite pores (free solvent). As expected, the melting temperature of trapped solvent decreases with average network chains density, i.e. from EPDM-1 to EPDM-3, as previously shown for a series of vulcanized Natural Rubber (NR). [48]

The two peak maxima of melting temperatures $T_{m,1}$ and $T_{m,2}$ slightly increase with applied stretching ratio, for EPDM-2, while only $T_{m,2}$ is increased for EPDM-3. A single peak maximum of the melting temperature in EPDM-1 is observed below T_m^0, but rapidly merges with free solvent melting because pore sizes reach the size of free solvent crystals, hence not possible to deconvolute. More strikingly, the intensity of the peak maximum at $T_{m,2}$ increases in detriment to the one of $T_{m,1}$ in both EPDM-2 and EPDM-3 with increased stretching ratio. These observations suggest an increase of pore size with applied deformation. However, their quantitative interpretation requires a deconvolution of melting profiles as discussed in the following.

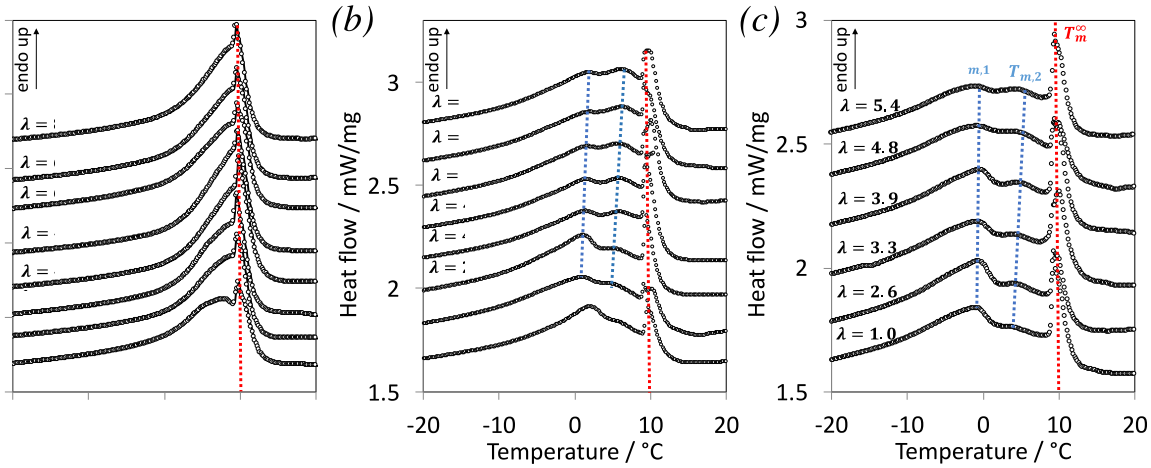

Figure 9. Heat flow versus temperature during heating for EPDM-1 *(a)*, EPDM-2 *(b)* and EPDM-3 *(c)*. Blue dotted lines represent the maximum peak intensity corresponding to melting of trapped solvent ($T_{m,1}$ and $T_{m,2}$) and red dotted lines show the free solvent melting peak.

DSC thermoporosimetry profiles in Figure 9 are translated into pore size distribution for EPDM-1, EPDM-2 and EPDM-3 via equations 9 and 10 detailed in section 2.4 (see also Supplementary Figure S4). The deduced normalized pore size L/L_f shows large distribution (Figure 10), consistent with previous NMR observations of network heterogeneities in filled vulcanized EPDM. [15,16]

Moreover, the higher the average network chain density, the smaller the pore size distribution. This traduces a homogenization of the network chains density, occurring by crosslinking of largest pore domains while small pore domains remain unchanged. The latter observation confirms similitude of local network densities in domains made of shortest chains (right side of the curves in Figure 10) in all vulcanized EPDM samples while average network chain density obtained by swelling (Table 1) or thermoporosimetry (dotted lines in Figure 10) varies.

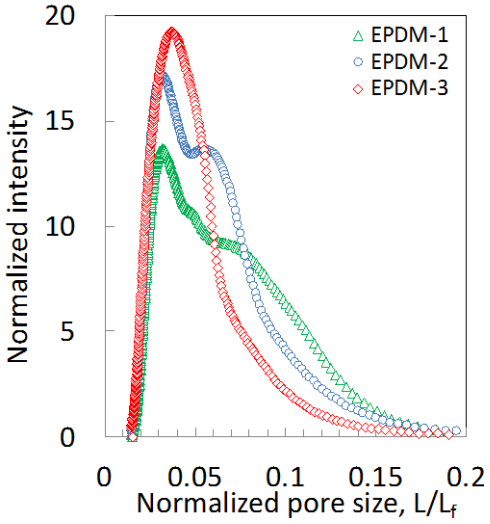

Figure 10. Normalized intensity versus normalized pore size giving access to pore size distribution in undeformed EPDM-1, EPDM-2 and EPDM-3. The procedure and equations used are detailed in section 2.4 of the manuscript. Dotted lines show the average normalized pore size equal to 0.070, 0.055, 0.048 for EPDM-0, EPDM-1 and EPDM-2 respectively. The average normalized pore sizes obtained for EPDM-1 and EPDM-2 are reported on Figure 11 at the corresponding axis value λ=1.

The averaged L/L_f is calculated for different specimens that have experienced loading at various stretching ratios (Figure 11a) and is found to follow different regimes: in the initial steps of deformation (λ<3) only weak pore size modification is observed. At higher deformation (λ>3), the pore size increases with λ. Such transition is concomitant to transition in rise of swelling ratio upon loading (Figure 7a), and with transition from reversible to irreversible volumetric strain (Figure 5a) that might indicate the large voiding size contributing to their irreversibility.

Finally, like for swelling experiments (Figure 7a and Figure 8a), the pore size levels off for the highest λ. This is due to the presence of pre-existing stable voids that are initially filled by the solvent without being swollen which underestimates the average values of pore size. Assuming equiaxial re-opening of cavities upon swelling, the characteristic distance of chains network *r* in the un-swollen state can be deduced from the pore size *L* through the relation:

$$L = Q^{1/3} r \tag{13}$$

In vulcanized rubber, *r* is the root-mean-square end-to-end distance $\sqrt{\langle R^2 \rangle}$ between nodes of the chains network. Assuming Gaussian chains statistics for the calculation of *r*, it comes:

$$\langle R^2 \rangle = C_\infty n l^2 \tag{14}$$

with $C_\infty = 6.62$ [49] is the number of backbone bonds in one EPDM statistical segment, *n* is the average number of backbone bonds per monomer unit and *l* =2 Å is the average main-chain bond length. $n = M/M_0$ with $M = \rho/\nu$ and M_0 =35 g.mol^{-1} the weight-average molar mass of the network chains and of the monomer respectively. ρ =0.865 g.cm^{-3} is the bulk rubbery density and ν (mol.cm^{-3}) is the network chains density (Table 1). The average distance between nodes of the chains network is then written:

$$r = \left(\frac{C_\infty \rho}{\nu M_0}\right)^{1/2} l \tag{15}$$

Calculated distances between nodes of the elastic network in the relaxed state are 4.2, 4.7 and 6.9 nm for EPDM-3, EPDM-2 and EPDM-1 respectively. From Eq. 11 and 13, the average swollen normalized pore size, deduced from the method proposed in section 2.4 and Figure S4, depends on the average crosslink density, following the relation:

$$\frac{L}{L_f} Q^{-1/3} = K\nu^{-1/2} \quad (16)$$

with K a constant equal to $(C_\infty \rho / M_0)^{1/2} l / L_f$. One might note that Gaussian approximation is used for developing Equation 16. Gaussian chains can be disturbed by the non-deformable filler particles dispersed in the elastomer matrix. [50] Here, assuming equiaxial reopening of the cavities upon swelling, Equation 2 adapted to swelling gives $\Delta Q/Q_0 = \lambda^3 - 1$. Hence, the maximum value of Q_r = 3.6 (Figure 7a) corresponds to λ = 1.66, which is close to λ range of Gaussian behaviour [1;1.5] as discussed in Figure 4b, suggesting the Gaussian assumption to be adapted to describe L-ν relationship. Equation 16 fits experimental data, with slope K defined in equation 16, in the full strain range of stretched EPDM-1 and EPDM-2 (Figure 11b) and thus verifies the increased damage with stretching ratio to be associated with increased void size at network chains scale.

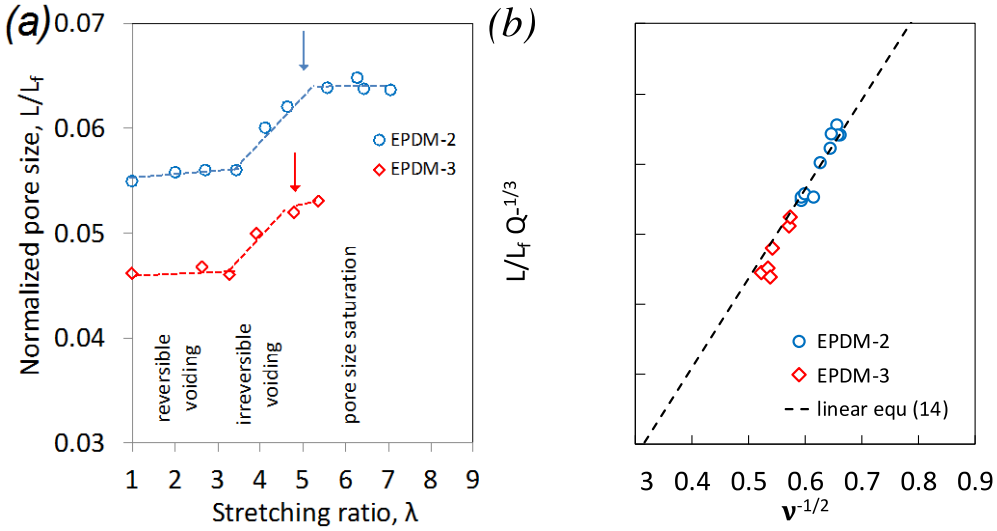

Figure 11. *(a)* Normalized average pore size deduced from the methodology detailed in Supplementary Figure S4 versus stretching ratio for EPDM-2 and EPDM-3. The series of thermoporosimetry experiments performed on EPDM-1 has too low network chain density so that associated pore sizes are in the range of pore sizes of the free solvent and melting peaks cannot be deconvoluted properly. *(b)* $L/L_f Q^{-1/3}$ versus $\nu^{-1/2}$ for EPDM-2 and EPDM-3. The dotted line is a regression fit $y=Kx$ of experimental data with a slope K=0.0637 and R squared value of 0.898.

To sum up, various deformation regimes corresponding to strain-induced damage mechanisms have been described for a series of carbon-black filled vulcanized/unvulcanized EPDM and related to damage at network chains scale.

In the low strain regime (λ<3), materials undergo reversible damage mechanisms. It is accompanied by reversible volumetric strain (Figure 5a), low permanent longitudinal deformation (Figure 5b), weak variation in swelling ratio (Figure 7a) and slow rise of swollen pore size (Figure 10a). Conformational changes that occur upon deformation can be argued to partly explain reversible volumetric strain. However, in the swollen state, polymer solvent interaction strongly influences chains conformation and might partially suppress the remaining chains conformation induced by mechanical loading, especially given the high swelling ratio values (Figure 7a). Slight increased swelling fraction and pore size are hence more related to localized, small and reversible voids which contribute to a slight increase in volumetric strain in the low deformation regime. Such voiding might be reflected by the damage of elastic network, as shown by a slight decrease in the network chains density in the initial steps of deformation (Figure 8). At such low deformations, pores sizes remain in the range of undamaged crosslinks distances (4-6 nm, cf. comments below equation 15). The chains network damage upon loading is associated with the loss of some network cross-links and the creation of dangling chains. Within the frame of the tube theory, [51] reduced topological constraints and eased relaxation of dangling chains during unloading favour reversible closing of small cavities via re-entanglement.

In higher strain regime (3<λ<5), irreversible damage is accompanied by permanent volumetric strain (Figure 5a), rise in permanent longitudinal deformation (Figure 5b), large increase of swelling ratio (Figure 7a) and large rise of pore size (Figure 10a). Plastic deformation in filled rubber might favour voiding stability. However, quite low absolute value of permanent

deformation upon unloading especially for the series vulcanized EPDM samples (Figure 5b), suggests plasticity not being the major cause for permanent voiding. The asymmetrical shape of the volumetric strain curves and high hysteresis (Figure 2c, Figure 4c, Supplementary Figure S1c-S3c) suggest opening and closing cavities to be intrinsically different mechanisms. Void nucleation is a kinetic mechanism which depends on experimental time. A void nucleus spontaneously grows up to a critical size upon stretching so that elastic strain energy is high enough to compensate newly created surface energy [52] and makes them thermally stable, even after the load release. [53] Kinetics of closing cavities contrarily relates to a return to equilibrium state between existing surface tension and strain energy. Thermoporosimetry does not provide absolute values for pore sizes and only average pore sizes have been analysed for sake of simplicity. However, such unambiguous transition at λ=3 in pore size is expected to ease transition from reversible to irreversible voids occurring at same λ.

At higher deformations, λ >5, both swelling ratio (arrows in Figure 7a, Figure 8a) and pore size (arrows in Figure 10a) reach threshold values, that we ascribe to the predominance of irreversible large voids that do not contribute to swelling behaviour. For surface energy of about 0.03 J/m^2 and for cavities of 100 nm, the effect of surface tension is negligible. [52] This size corresponds to the range of filler particles size observed by SEM (Figure 6b). Hence, such particle decohesion would yield in stable voiding. We thus suggest that, for λ >5, additionally to voiding occurring in the rubber matrix constrained between filler aggregates, damage is also expected to be accelerated by the nucleation of large cavity sites initiated by the decohesion of rigid filler and cluster that grow into the rubber matrix before yielding to macroscopic failure.

4. Conclusion

Due to strain amplification in rubber matrix and stress localization at filler/rubber and filler/cluster interfaces, vulcanized filled rubbers exhibit significant damage mechanisms when deformed up to failure, as shown in this paper on a series of EPDM samples. The observation of large voiding volume fraction however suggests such damage being not only localized at the interfaces but also to develop into the rubber matrix, necessarily accompanied by a significant modification of the rubber chains network. To account for this, we developed an experimental method to identify the relationship between damage classically observed at macro-scale and alteration of elastically active chains network. Voids fraction measured via Digital Image Correlation (DIC) and Flory-Rehner equation have been combined to estimate *in situ*, i.e. during mechanical testing, the modification of network chains density, ν. From this approach, two strain regimes have been identified: (i) at λ <3, reversible voiding is accompanied with slight decrease of ν and (ii) at λ >3 voiding becomes irreversible and ν significantly decrease with strain. We propose then, as revealed by *ex situ* thermoporosimetry, the transition from reversible to irreversible regime to be dominated by increased void sizes of rubber network domains ensuring their thermal stability. It could be of interest in future works to corroborate this by *in situ* measurements combining micro-computed tomography (µCT) and Small Angle X-Ray Scattering (SAXS) to access the full pore size distribution. We finally show that DIC can be easily used to monitor the progress of network chains damage during the uniaxial deformation of rubber systems. It could be profitable to generalize the understanding of molecular mechanisms at the origin of macroscopic damage in rubber systems, not only under single uniaxial tension, but in more industrially processes such as mechanical devulcanization, irradiation of electric cables, dynamic crack propagation in tires.

5. Acknowledgements

The authors are indebted to the company SACRED for providing and processing of the rubber gum and to the laboratory GEPEA of the University of Nantes for the detailed set up of the curing procedure of rubber materials. This work was performed within the framework of the project ECOTHER supported by BPiFrance.

6. References

1. Noordermeer, J. W. M. Ethylene–Propylene Elastomers. *Encycl. Polym. Sci. Technol.* (2002). doi:10.1002/0471440264.pst125
2. Young, D. G. Dynamic Property and Fatigue Crack Propagation Research on Tire Sidewall and Model Compounds. *Rubber Chem. Technol.* **58**, 785–805 (1985).
3. Sahakaro, K., Naskar, N., Datta, R. N. & Noordermeer, J. W. M. Blending of NR/BR/EPDM by reactive processing for tire sidewall applications. I. Preparation, cure characteristics and mechanical properties. *J. Appl. Polym. Sci.* **103**, 2538–2546 (2007).
4. De Almeida, A., Chazeau, L., Vigier, G., Marque, G. & Goutille, Y. Influence of PE/PP ratio and ENB content on the degradation kinetics of γ-irradiated EPDM. *Polym. Degrad. Stab.* **110**, 175–183 (2014).
5. Fisher J.F. Method of devulcanizing a cross-linked elastomeric material U.S. Patent Application No 13/304,509, (2013).
6. Diaz, R., Colomines, G., Peuvrel-Disdier, E., & Delterre, R. Thermo-mechanical recycling of rubber: Relationship between material properties and specific mechanical energy. Journal of Materials Processing Technology, **252**, 454-468. (2018).

7. Chrysochoos, A. *et al.* Use of Full-Field Digital Image Correlation and Infrared Thermography Measurements for the Thermomechanical Analysis of Material Behaviour. *Strain* **46**, 117–130 (2010).
8. Maurel-Pantel, A., Baquet, E., Bikard, J., Bouvard, J. L. & Billon, N. A thermo-mechanical large deformation constitutive model for polymers based on material network description: Application to a semi-crystalline polyamide 66. *Int. J. Plast.* **67**, 102–126 (2015).
9. Samaca Martinez, J. R., Balandraud, X., Toussaint, E., Le Cam, J.-B. & Berghezan, D. Thermomechanical analysis of the crack tip zone in stretched crystallizable natural rubber by using infrared thermography and digital image correlation. *Polymer* **55**, 6345–6353 (2014).
10. Le Cam, J.-B. A review of volume changes in rubbers: the effect of stretching. *Rubber Chem. Technol.* **83**, 247–269 (2010).
11. Ramier, J. *et al.* In situ SALS and volume variation measurements during deformation of treated silica filled SBR. *J. Mater. Sci.* **42**, 8130–8138 (2007).
12. Montesano, J., Fawaz, Z. & Bougherara, H. Use of infrared thermography to investigate the fatigue behavior of a carbon fiber reinforced polymer composite. *Compos. Struct.* **97**, 76–83 (2013).
13. Hamed, G. R. Energy Dissipation and the Fracture of Rubber Vulcanizates. *Rubber Chem. Technol.* **64**, 493–500 (1991).
14. Samaca Martinez, J. R., Le Cam, J.-B., Balandraud, X., Toussaint, E. & Caillard, J. Filler effects on the thermomechanical response of stretched rubbers. *Polym. Test.* **32**, 835–841 (2013).
15. Valentin, J. L. *et al.* Inhomogeneities and Chain Dynamics in Diene Rubbers Vulcanized with Different Cure Systems†. *Macromolecules* **43**, (2010).

16. Litvinov, V., A. Orza, R., Klueppel, M., Duin, M. & Magusin, P. Rubber–Filler Interactions and Network Structure in Relation to Stress–Strain Behavior of Vulcanized, Carbon Black Filled EPDM. *Macromolecules* **44**, 4887–4900 (2011).
17. Diani, J., Fayolle, B. & Gilormini, P. A review on the Mullins effect. *Eur. Polym. J.* 601–612 (2009).
18. Houwink, R. Slipping of Molecules during the Deformation of Reinforced Rubber. *Rubber Chem. Technol.* **29**, 888–893 (1956).
19. Merckel Yannick, Diani Julie, Brieu Mathias & Caillard Julien. Effects of the amount of fillers and of the crosslink density on the mechanical behavior of carbon-black filled styrene butadiene rubbers. *J. Appl. Polym. Sci.* **129**, 2086–2091 (2013).
20. Zhang, H. *et al.* Nanocavitation in Carbon Black Filled Styrene–Butadiene Rubber under Tension Detected by Real Time Small Angle X-ray Scattering. *Macromolecules* **45**, (2012).
21. Le Cam, J.-B., Huneau, B., Verron, E. & Gornet, L. Mechanism of fatigue crack growth in carbon black filled natural rubber. *Macromolecules* **37**, 5011–5017 (2004).
22. Dannenberg, E. M. & Brennan, J. J. Strain Energy as a Criterion for Stress Softening in Carbon-Black-Filled Vulcanizates. *Rubber Chem. Technol.* **39**, 597–608 (1966).
23. Kraus, G., Childers, C. W. & Rollmann, K. W. Stress softening in carbon black-reinforced vulcanizates. Strain rate and temperature effects. *J. Appl. Polym. Sci.* **10**, 229–244 (1966).
24. Mullins, L. & Tobin, N. R. Carbon-Black Loaded Rubber Vulcanizates: Volume Changes in Stretching. *Rubber Chem. Technol.* **31**, 505–512 (1958).
25. Melnikov, A. Y. & Leonov, A. I. Damage of Cross-Linked Rubbers as the Scission of Polymer Chains: Modeling and Tensile Experiments. *ArXiv11080579 Cond-Mat* (2011).

26. Govindjee, S. & Simo, J. A micro-mechanically based continuum damage model for carbon black-filled rubbers incorporating Mullins' effect. *J. Mech. Phys. Solids* **39**, 87–112 (1991).
27. Marckmann, G. *et al.* A theory of network alteration for the Mullins effect. *J. Mech. Phys. Solids* **50**, 2011–2028 (2002).
28. Hamed, G. R. Molecular Aspects of the Fatigue and Fracture of Rubber. *Rubber Chem. Technol.* **67**, 529–536 (1994).
29. Vic-3D (2007) ®Software. Correlated Solutions Incorporated, Columbia, S. https://www.correlatedsolutions.com/vic-3d/.
30. Candau, N. Pradille, C. Bouvard, J-L. & Billon, N. On the use of a four-cameras stereovision system to characterize large 3D deformation in elastomers. *Polym. Test.* **56**, 314-320. (2016).
31. De Crevoisier, J. *et al.* Volume changes in a filled elastomer studied via digital image correlation. *Polym. Test.* **31**, 663–670 (2012).
32. Flory, P. J. & Jr, J. R. Statistical Mechanics of Cross-Linked Polymer Networks I. Rubberlike Elasticity. *J. Chem. Phys.* **11**, 512–520 (1943).
33. Kraus, G. Swelling of filler-reinforced vulcanizates. *J. Appl. Polym. Sci.* **7**, 861–871 (1963).
34. Candau, N. *et al*. Strain-Induced Crystallization of Natural Rubber and Cross-Link Densities Heterogeneities. *Macromolecules*. **47**(16), 5815-5824. (2014).
35. Ren, Y. *et al.* Effects of plasticizers on the strain-induced crystallization and mechanical properties of natural rubber and synthetic polyisoprene. *RSC Adv.* **5**, 11317–11324 (2015).
36. Mark, J. E. The effect of strain-induced crystallization on the ultimate properties of an elastomeric polymer network. *Polym. Eng. Sci.* **19**, 409–413 (1979).

37. Ramier, J. Mechanical behaviour of filled elastomers, the influence of filler adhesion to polymer and the influence of morphology. PhD Dissertation, Institut national des sciences appliquées de Lyon. (2004).
38. Kost, J., Narkis, M. & Foux, A. Resistivity behavior of carbon-black-filled silicone rubber in cyclic loading experiments. *J. Appl. Polym. Sci.* **29**, 3937–3946 (1984).
39. Le Cam, J.-B. & Toussaint, E. Cyclic volume changes in rubber. *Mech. Mater.* **41**, 898–901 (2009).
40. Omnès, B., Thuillier, S., Pilvin, P., Grohens, Y. & Gillet, S. Effective properties of carbon black filled natural rubber: Experiments and modeling. *Compos. Part Appl. Sci. Manuf.* **39**, 1141–1149 (2008).
41. Hertz, D. Theory & Practice Of Vulcanization. *Elastomerics.* **116**(11), 17-21. (1984).
42. Dijkhuis, K. A. J., Noordermeer, J. W. M. & Dierkes, W. K. The relationship between crosslink system, network structure and material properties of carbon black reinforced EPDM. *Eur. Polym. J.* **45**, 3302–3312 (2009).
43. Kucherskii, A. M. New characteristic of tensile stress–strain properties in rubbers. *Polym. Test.* **22**, 503–507 (2003).
44. Gent, A. N. & Lindley, P. B. Internal Rupture of Bonded Rubber Cylinders in Tension. *Proc. R. Soc. Math. Phys. Eng. Sci.* **249**, 195–205 (1959).
45. Valentín, J. L., Carretero-González, J., Mora-Barrantes, I., Chassé, W. & Saalwächter, K. Uncertainties in the Determination of Cross-Link Density by Equilibrium Swelling Experiments in Natural Rubber. *Macromolecules* **41**, 4717–4729 (2008).

46. Litvinov, V. M., Barendswaard, W. & van Duin, M. The Density of Chemical Crosslinks and Chain Entanglements in Unfilled EPDM Vulcanizates as Studied with Low Resolution, Solid State 1H NMR. *Rubber Chem. Technol.* **71**, 105–118 (1998).
47. Flory, P.J. Principles of Polymer Chemistry. Cornell University (1953).
48. Candau et al. Complex dependence on the elastically active chains density of the strain induced crystallization of vulcanized natural rubbers, from low to high strain rate. *Polymer*. **97**, 158-166 (2016).
49. Richter, D. *et al.* On the origins of entanglement constraints. *Macromolecules* **26**, 795–804 (1993).
50. Heinrich, G., Klüppel, M. & Vilgis, T. A. Reinforcement of elastomers. *Curr. Opin. Solid State Mater. Sci.* **6**, 195–203 (2002).
51. Edwards, S.F, Vilgis, T.A. The tube model theory of rubber elasticity. Reports on Progress in Physics. **51**(2), 243. (1988).
52. Fond, C. Cavitation criterion for rubber materials: A review of void-growth models. *J. Polym. Sci. Part B Polym. Phys.* **39**, 2081–2096 (2001).
53. Diani, J. Irreversible growth of a spherical cavity in rubber-like material: A fracture mechanics description. *Int. J. Fract.* **112**, 151–161 (2001).